Generation of Bimaternal and Bipaternal Mice from Hypomethylated Haploid ESCs with Imprinting Region Deletions

Article *in* Cell stem cell · November 2018

DOI: 10.1016/j.stem.2018.09.004

CITATIONS
7

READS
355

15 authors, including:

Leyun Wang
Chinese Academy of Sciences
15 PUBLICATIONS **96** CITATIONS
SEE PROFILE

Guihai Feng
Chinese Academy of Sciences
37 PUBLICATIONS **659** CITATIONS
SEE PROFILE

Liu Chao
Chinese Academy of Sciences
8 PUBLICATIONS **79** CITATIONS
SEE PROFILE

Haifeng Wan
Chinese Academy of Sciences
175 PUBLICATIONS **1,246** CITATIONS
SEE PROFILE

Article

Cell Stem Cell

Generation of Bimaternal and Bipaternal Mice from Hypomethylated Haploid ESCs with Imprinting Region Deletions

Graphical Abstract

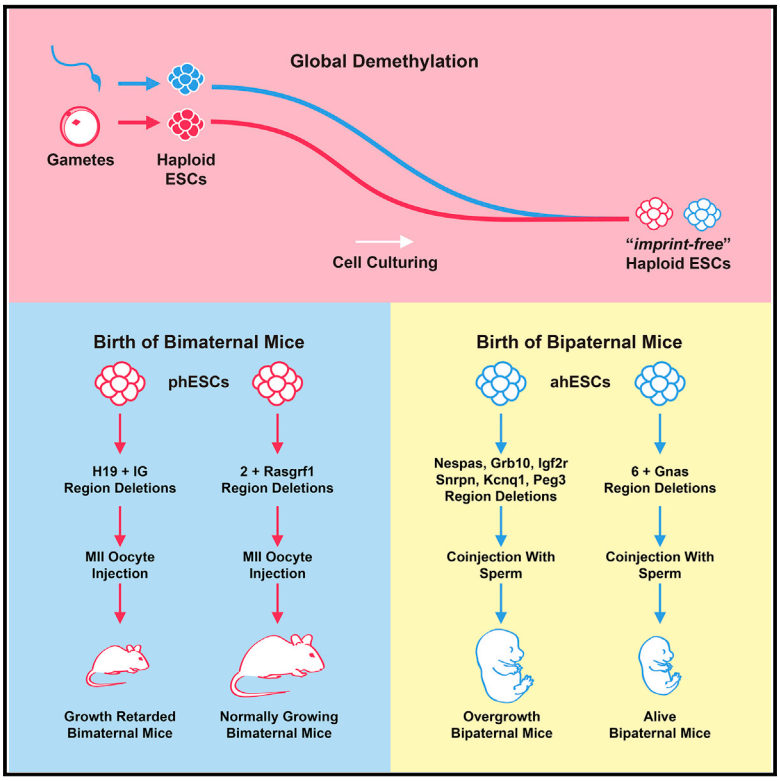

Highlights

- Haploid ESCs display PGC-like methylation profiles following *in vitro* cultivation
- Parthenogenetic and androgenetic haploid ESCs show different demethylation dynamics
- phESCs carrying 3 deleted imprinted regions support normal growth of bimaternal mice
- ahESCs carrying 7 deleted imprinted regions produce live full-term bipaternal mice

Authors

Zhi-Kun Li, Le-Yun Wang, Li-Bin Wang, ..., Wei Li, Qi Zhou, Bao-Yang Hu

Correspondence

liwei@ioz.ac.cn (W.L.), qzhou@ioz.ac.cn (Q.Z.), byhu@ioz.ac.cn (B.-Y.H.)

In Brief

Li et al. utilize haploid ESCs to overcome the uniparental reproductive barriers in mice. They found parent-specific erasure of DNA methylation between parthenogenetic and androgenetic haploid ESCs. After combining gametes and hypomethylated haploid ESCs with certain imprinted region deletions, the authors generated normally growing bimaternal mice and live bipaternal mice.

Li et al., 2018, Cell Stem Cell *23*, 665–676
November 1, 2018
https://doi.org/10.1016/j.stem.2018.09.004

CellPress

Cell Stem Cell
Article

Generation of Bimaternal and Bipaternal Mice from Hypomethylated Haploid ESCs with Imprinting Region Deletions

Zhi-Kun Li,[1,2,5] Le-Yun Wang,[1,2,5] Li-Bin Wang,[1,2,3,5] Gui-Hai Feng,[1,2,5] Xue-Wei Yuan,[1,2,4,5] Chao Liu,[1,2,3] Kai Xu,[1,2,3] Yu-Huan Li,[1,2,3] Hai-Feng Wan,[1,2] Ying Zhang,[1,2] Yu-Fei Li,[1,2,3] Xin Li,[1,2] Wei Li,[1,2,3,*] Qi Zhou,[1,2,3,6,*] and Bao-Yang Hu[1,2,3,*]

[1]State Key Laboratory of Stem Cell and Reproductive Biology, Institute of Zoology, Chinese Academy of Sciences, Beijing 100101, China
[2]Institute for Stem Cell and Regeneration, Chinese Academy of Sciences, Beijing 100101, China
[3]University of the Chinese Academy of Sciences, Beijing 100049, China
[4]College of Life Science, Northeast Agricultural University, Harbin 150030, China
[5]These authors contributed equally
[6]Lead Contact
*Correspondence: liwei@ioz.ac.cn (W.L.), qzhou@ioz.ac.cn (Q.Z.), byhu@ioz.ac.cn (B.-Y.H.)
https://doi.org/10.1016/j.stem.2018.09.004

SUMMARY

Unisexual reproduction is widespread among lower vertebrates, but not in mammals. Deletion of the H19 imprinted region in immature oocytes produced bimaternal mice with defective growth; however, bipaternal reproduction has not been previously achieved in mammals. We found that cultured parthenogenetic and androgenetic haploid embryonic stem cells (haESCs) display DNA hypomethylation resembling that of primordial germ cells. Through MII oocyte injection or sperm coinjection with hypomethylated haploid ESCs carrying specific imprinted region deletions, we obtained live bimaternal and bipaternal mice. Deletion of 3 imprinted regions in parthenogenetic haploid ESCs restored normal growth of fertile bimaternal mice, whereas deletion of 7 imprinted regions in androgenetic haploid ESCs enabled production of live bipaternal mice that died shortly after birth. Phenotypic analyses of organ and body size of these mice support the genetic conflict theory of genomic imprinting. Taken together, our results highlight the factors necessary for crossing same-sex reproduction barriers in mammals.

INTRODUCTION

Reproduction by parthenogenesis or gynogenesis is widespread among vertebrates such as reptiles, fish, and amphibians but does not exist in mammals (Neaves and Baumann, 2011). In the 1980s, elegant pronuclear transplantation experiments performed by the Solter and Surani laboratories suggested that mouse development required both maternal and paternal contributions, which implied the presence of genetic asymmetries of two parental chromosomes (Barton et al., 1984; McGrath and Solter, 1983, 1984; Surani and Barton, 1983; Surani et al., 1984).

To study the genetic asymmetries on chromosomes, Cattanach, Searle, and colleagues analyzed offspring with uniparental disomies for specific regions that were generated by mating mice that were heterozygous for Robertsonian or balanced translocations (Cattanach and Kirk, 1985; Searle and Beechey, 1978). The uniparental duplications, resulting in severe embryonic defects or lethality, are distributed over seven chromosomes as 11 segments: proximal and distal chromosome 2 (chr2); proximal chr6; proximal, central, and distal chr7; proximal chr11; distal chr12; proximal and distal chr17; and proximal chr18 (Berger and Epstein, 1989; Cattanach, 1986; Cattanach et al., 1996; Cattanach and Jones, 1994; Cattanach and Kirk, 1985; Cattanach and Rasberry, 1993; Johnson, 1974; Searle and Beechey, 1978, 1990). A decade after the first genetic experiment, three imprinted genes were identified by molecular characterization of the genetic asymmetrical chromosome regions (Barlow et al., 1991; Bartolomei et al., 1991; Ferguson-Smith et al., 1991). To date, approximately 100 imprinted genes have been described in mammals (Bartolomei and Ferguson-Smith, 2011).

The genetic asymmetries between parental genomes are also the subject of genetic conflict theory. This concept proposes that paternally inherited imprinted genes "extract" nutrients from the mother during gestation. By contrast, maternally inherited genes counteract the effect of paternal genes (Constância et al., 2004; Wilkins and Haig, 2003). The differences between parental genomes, including genomic imprinting, underlie the uniparental reproduction barriers of mammals and promote the beneficial exchange of genetic information, the spread of evolutionarily advantageous mutations, and the maintenance of competitiveness in offspring (Wilkins and Haig, 2003).

Using immature oocytes with a deletion of the H19 imprinted region, Kono et al. (2004) produced the first mice from two mothers, proving the importance of genomic imprinting in hindering parthenogenesis. However, many of the barriers to uniparental reproduction have not been revealed. For example, the Dlk1-Dio3 imprinted region inherited from the father is essential for biparental embryo development (Constância et al., 2004;

Georgiades et al., 2000) but dispensable for the bimaternal embryo (Kono et al., 2004). Global epigenetic investigation of immature oocytes is needed to understand these bimaternal reproduction barriers. However, the heterogeneous character of immature oocytes has limited such studies (Hiura et al., 2006). Accordingly, bipaternal reproduction, which has only been found in specific fish (Corley-Smith et al., 1996), has not been achieved in mammals until now.

Haploid embryonic stem cells (haESCs) have been successfully generated in mice, rats, monkeys, and humans (Leeb and Wutz, 2011; Li et al., 2014; Sagi et al., 2016; Yang et al., 2013) and have provided new platforms for genetic screening and animal production (Li et al., 2012, 2014; Sagi et al., 2016; Yang et al., 2012). Previously, we produced bimaternal mice by injecting parthenogenetic haploid ESCs (phESCs) with deletions of the H19 and Dlk-Dio2 intergenic region (IG) imprinted regions into MII oocytes and demonstrated the indispensability of the IG deletion (Li et al., 2016). By further characterization of haploid ESCs, we aim to determine why some deletions are sufficient to cross bimaternal reproduction barriers in mammals. We also investigated mechanisms preventing bipaternal reproduction and successfully mitigated the identified imprinting blocks to generate full-term bipaternal mice.

RESULTS

Hypomethylation in Haploid ESCs Mimics Features of Reprogramming PGCs

First we performed reduced representation bisulfite sequencing (RRBS) for a global methylation analysis of androgenetic haploid ESCs (ahESCs, ~passage 20 and 40) and phESCs (~passage 20 and 40) (Figure 1A). The haploid ESCs exhibited global hypomethylation compared with oocyte, sperm, and tail tip fibroblasts (TTFs) (Figure 1B). At the chromosomal level, the methylation patterns of haploid ESCs were similar to those of embryonic day 10.5 (E10.5) primordial germ cells (PGCs), which had started global demethylation (Figure S1A; Kobayashi et al., 2013). Next we measured the average methylation levels at various genomic elements, including promoters, long interspersed nuclear elements (LINEs), short interspersed nuclear elements (SINEs), long terminal repeats (LTRs), enhancers, and imprinted regions. The methylation levels of promoters, LINEs, SINEs, LTRs, and enhancers of haploid ESCs were similar to those of E10.5 PGCs (Figures 1C and S1B; Kobayashi et al., 2013). In particular, the imprinted regions that were demethylated in PGCs exhibited a low methylation level in haploid ESCs, similar to E13.5 PGCs (Figures 1C and 1D; Kobayashi et al., 2013). On the contrary, the intracisternal A-particle element (IAP), a demethylation-resistant component in PGCs (Lane et al., 2003), was maintained in haploid ESCs (Figure S1B). Additionally, PGC-specific promotors showed similar hypomethylation patterns between haploid ESCs and PGCs (Figure S1C; Guo et al., 2017).

Notably, the RRBS results also revealed that global hypomethylation and loss of imprint occurred earlier in phESCs (approximately passage 20) than in ahESCs (approximately passage 40) (Figures 1B and 1D). Bisulfite sequencing results also confirmed loss of imprints in early-passage phESCs (passage 20) but not in ahESCs (passage 24) (Figure 1E). Additional bisulfite sequencing analyses suggested different loss-of-imprint dynamics in phESCs and ahESCs (Figures S1D and S1E). To interrogate the differences, we performed principal-component analysis (PCA) with all related samples. The result showed that both the early- and late-passage phESCs as well as the late-passage ahESCs were clustered with hypomethylated PGCs, whereas the early-passage ahESCs were clustered with sperm and TTFs (Figure 1F). The loss of DNA methylation occurred more rapidly in phESCs than in ahESCs, suggesting unknown differences in sperm and oocyte inherited genomes under naive ESC culture.

The hypomethylated ahESCs and phESCs presented a dome-shaped morphology, expressed typical pluripotency markers, and formed teratomas containing all three germ layers following subcutaneous injection into mice with severe combined immunodeficiency (SCID) (Figures S2A–S2F). The hypomethylated haploid ESCs could generate germline-transmitted chimeric mice after injection into blastocysts, suggesting unimpaired pluripotency (Figures S2G and S2H). Collectively, we found that phESCs and ahESCs exhibited PGC-like demethylation processes with different dynamics.

Production of Normal Bimaternal Mice with Hypomethylated phESCs

Previously, using homologous recombination, we introduced two deleted regions in phESCs and produced bimaternal mice (referred to as 2KO-bimaternal mice) by injection into MII oocytes (Figure 2A; Li et al., 2016). The cells were used after prolonged *in vitro* cultivation (~40 passages) and were expected to display the PGC-like hypomethylation status.

We reported retardation of growth in juvenile 2KO-bimaternal mice (Li et al., 2016). The adult 2KO-bimaternal mice exhibited a slower velocity and shorter moving distance in the open field test (Figures 2B and 2C). To understand these behavioral abnormalities, we compared the brain transcriptome of 2KO-bimaternal mice with the control and found 3 differentially imprinted genes: *Th*, *Xlr3b*, and *Rasgrf1* (Figures 2D and S2I). The *Th* mutation caused hypoactivity (Zhou and Palmiter, 1995), whereas changes in *Xlr3b* expression affected cognition (Davies et al., 2005). *Rasgrf1* expression affected olfactory learning and memory (Drake et al., 2011). Thus, all three genes had the potential to cause behavioral abnormalities when dysregulated. Impressively, the 2KO-bimaternal mice also exhibited longer lifespans than the control mice (Figure 2E). To understand the increased longevity, we tested metabolism-related factors in 2KO-bimaternal mice. A negative regulator of human lifespan, *Igf1*, was found to be decreased in bimaternal mice (Figure 2F; Suh et al., 2008). Additionally, the cholesterol level of these mice was found to be lower in serum biochemical tests (Figure 2G; Table S1). The above abnormalities in 2KO-bimaternal mice suggest the presence of postnatal developmental barriers in bimaternal reproduction.

Among the 3 differential genes in 2KO-bimaternal mice, *Rasgrf1* was consistent between neonates and adults (Figures 2D and S2I). We have also reported hypomethylation of the Rasgrf1 imprinted region in wild-type phESC-derived bimaternal embryos, which could develop up to E13.5 (Li et al., 2016). Accordingly, the Rasgrf1 imprinted region was hypomethylated in 2KO-bimaternal mice, early-passage phESCs,

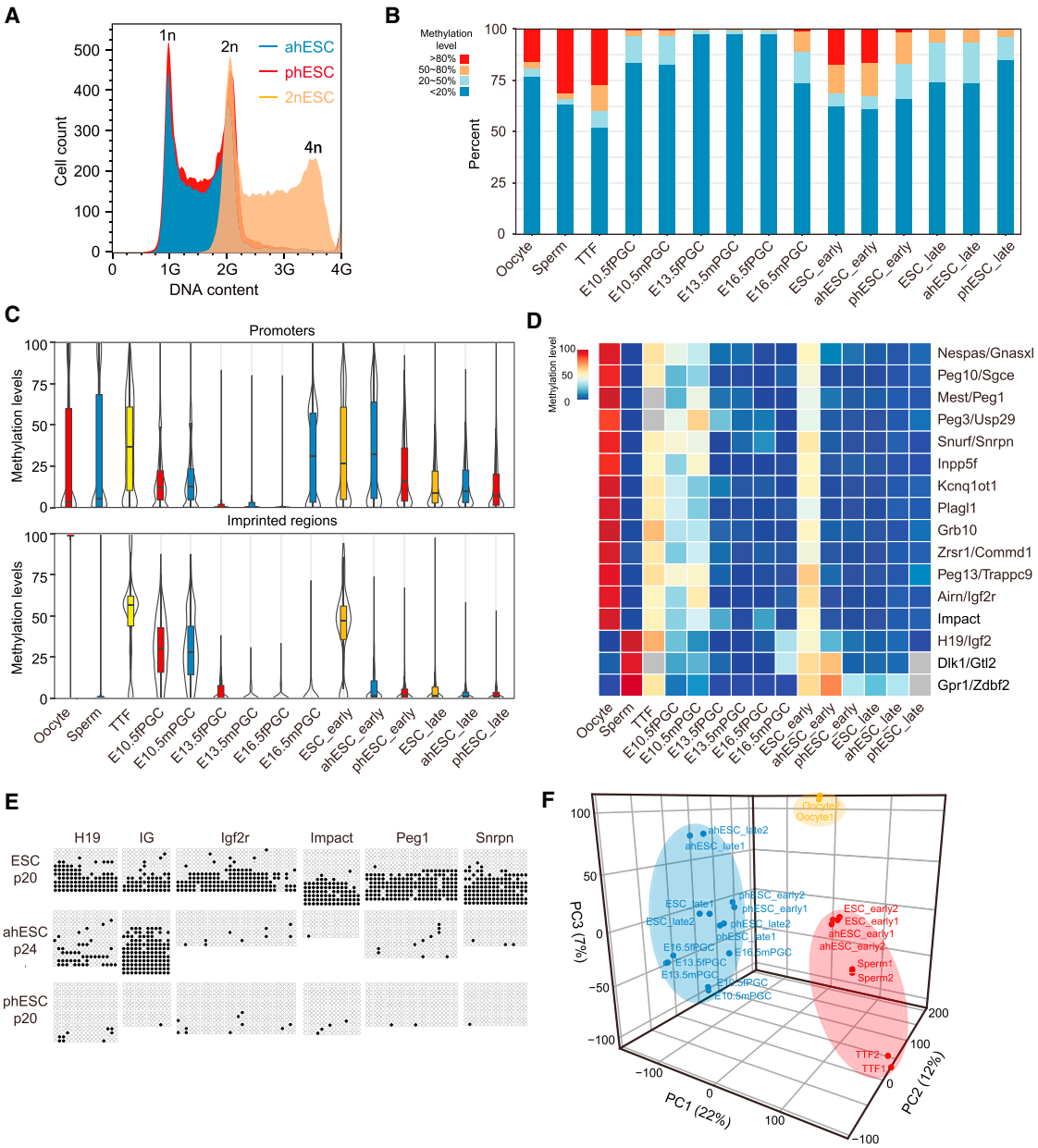

Figure 1. PGC-like Hypomethylation Characteristics of Haploid ESCs

(A) Fluorescence-activated cell sorting (FACS) analysis of the DNA content of phESCs and ahESCs. Diploid ESCs were stained as control.

(B) Distribution of DNA methylation levels in oocytes, sperm, TTFs, E10.5fPGCs (female PGCs at E10.5), E10.5mPGCs (male PGCs at E10.5), E13.5fPGCs (female PGCs at E13.5), E13.5mPGCs (male PGCs at E13.5), E16.5fPGCs (female PGCs at E16.5), E16.5mPGCs (male PGCs at E16.5), early-passage ESCs (passage 20, n = 2), early-passage ahESCs (passage 20, n = 2), early-passage phESCs (passages 19 and 20), late-passage ESCs (passage 42, n = 2), late-passage ahESCs (passages 40 and 42), and late-passage phESCs (passage 40, n = 2).

(C) DNA methylation levels at promoters (top) and imprinted regions (bottom) in all related samples.

(D) Heatmap of imprinted region methylation in all related samples. Gray squares indicate a lack of valid reads.

(E) Bisulfite sequencing analysis of imprinted regions at the H19, IG, Igf2r, Impact, Peg1, and Snrpn loci in ESCs (passage 20), ahESCs (passage 24), and phESCs (passage 20). Filled circles represent methylated cytosines, and open circles represent unmethylated cytosines.

(F) Principal-component analyses of the CpG methylation levels in all related samples covered with no less than 10 reads. Each sample has two independent repeats. PC1, PC2, and PC3 represent the top three principal components. Three groups were determined by unsupervised k-means clustering.

See also Figures S1 and S2.

and late-passage ahESCs (Figure 2H). Thus, we generated 3KO-phESCs by deleting the H19, IG, and Rasgrf1 imprinted regions by CRISPR-Cas9 in phESCs (approximately passage 24) (Figures 3A and S2J–S2N; Table S2) and successfully derived bimaternal pups by MII oocyte injection (Figures 3B and 3C). Notably, the 3KO-phESCs produced 29 (~14%) live

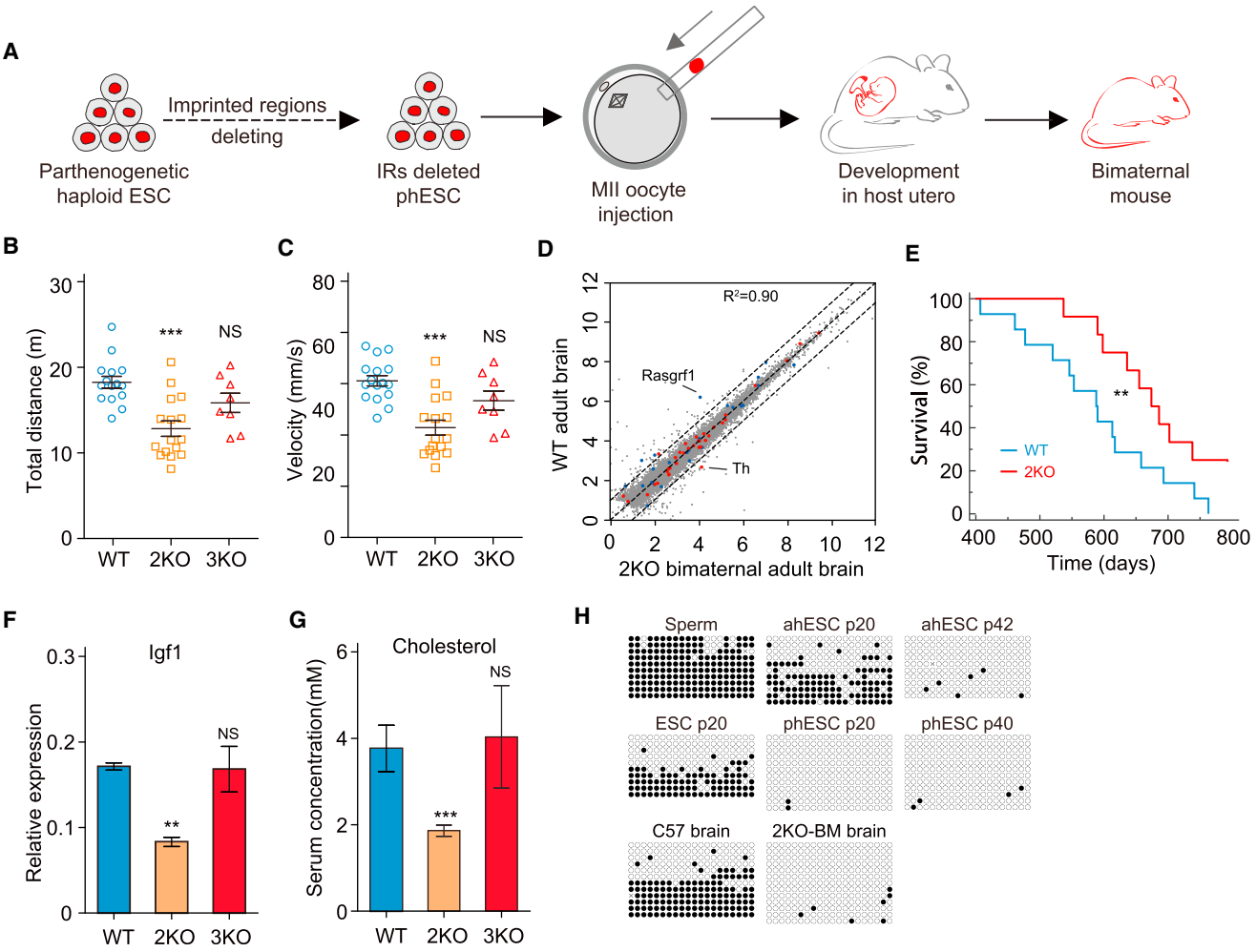

Figure 2. Abnormalities of Bimaternal Mice Generated with Hypomethylated phESCs

(A) Schematic of the generation of bimaternal mice by oocyte injection of phESCs carrying imprinted region deletions. IR, imprinted region.

(B) The movement distances of WT (n = 16), 2KO-bimaternal (n = 16), and 3KO-bimaternal (n = 8) mice.

(C) The movement velocities of 2KO-bimaternal mice (n = 16), 3KO-bimaternal mice (n = 8), and WT mice (n = 16).

(D) Scatterplot comparison of 2KO-bimaternal and WT adult brain transcriptomes. Pearson's correlation (R^2) was determined by Pearson's correlation.

(E) Kaplan-Meier survival curves of 2KO-bimaternal mice (n = 15) and genotype- and sex-matched wild-type controls (n = 14).

(F) Quantitative PCR analysis of *Igf1* in WT and bimaternal pup livers.

(G) Serum concentration of cholesterol in sera of WT and 2KO- and 3KO-bimaternal pups.

(H) Bisulfite sequencing analysis of Rasgrf1 imprinted regions in sperm, ahESCs (passages 20 and 42), diploid ESCs (passage 20), phESCs (passages 20 and 40), C57BL/6 adult mouse brain, and 2KO-bimaternal mouse brain. Filled circles represent methylated cytosines, and open circles represent unmethylated cytosines.

For all graphs, data are presented as mean ± SEM. **p < 0.01, ***p < 0.001. NS, not significant. See also Figure S2.

mice (referred to as 3KO-bimaternal mice) from 210 transferred embryos with an efficiency similar to that of round sperm (Table 1). The body (1.36 ± 0.78 g, n = 10) and placenta weights (0.11 ± 0.0056 g, n = 14) were normal (Figures S2O and S2P), and the *Rasgrf1* expression level was recovered in these mice (Figure 3D). Unexpectedly, global transcriptome analysis showed that all detected imprinted genes were regularly expressed (Figure 3E). Consistent with this observation, the behaviors and growth curve of these mice were normalized (Figures 2B, 2C, 3F, and 3G). Additionally, all serum biochemical parameters and *Igf1* expression were also normal in the 3KO-bimaternal mice (Figures 2F and 2G; Table S1).

The RRBS analysis showed that the global methylation level of 3KO-bimaternal embryo and brain were similar to the wild-type (WT) (Figure 3H). Notably, the imprinted regions in bimaternal embryo and brain were comparable with the WT, except for the H19 imprinted region, which was demethylated for the absence of paternal inherited imprints (Figure 3I). To examine fertility, female 3KO-bimaternal mice were mated with WT males. A total of 22 pups were delivered in 6 litters. Nine pups carrying the IG or H19 deletion died after birth, and the other 13 mice grew into adults (Table S3). To calculate the actual litter size of 3KO-bimaternal mice, the numbers of viable pups (WT and Rasgrf1$^{-/+}$) in each litter were multiplied by 4 according to the Mendelian ratio and compared with the litter

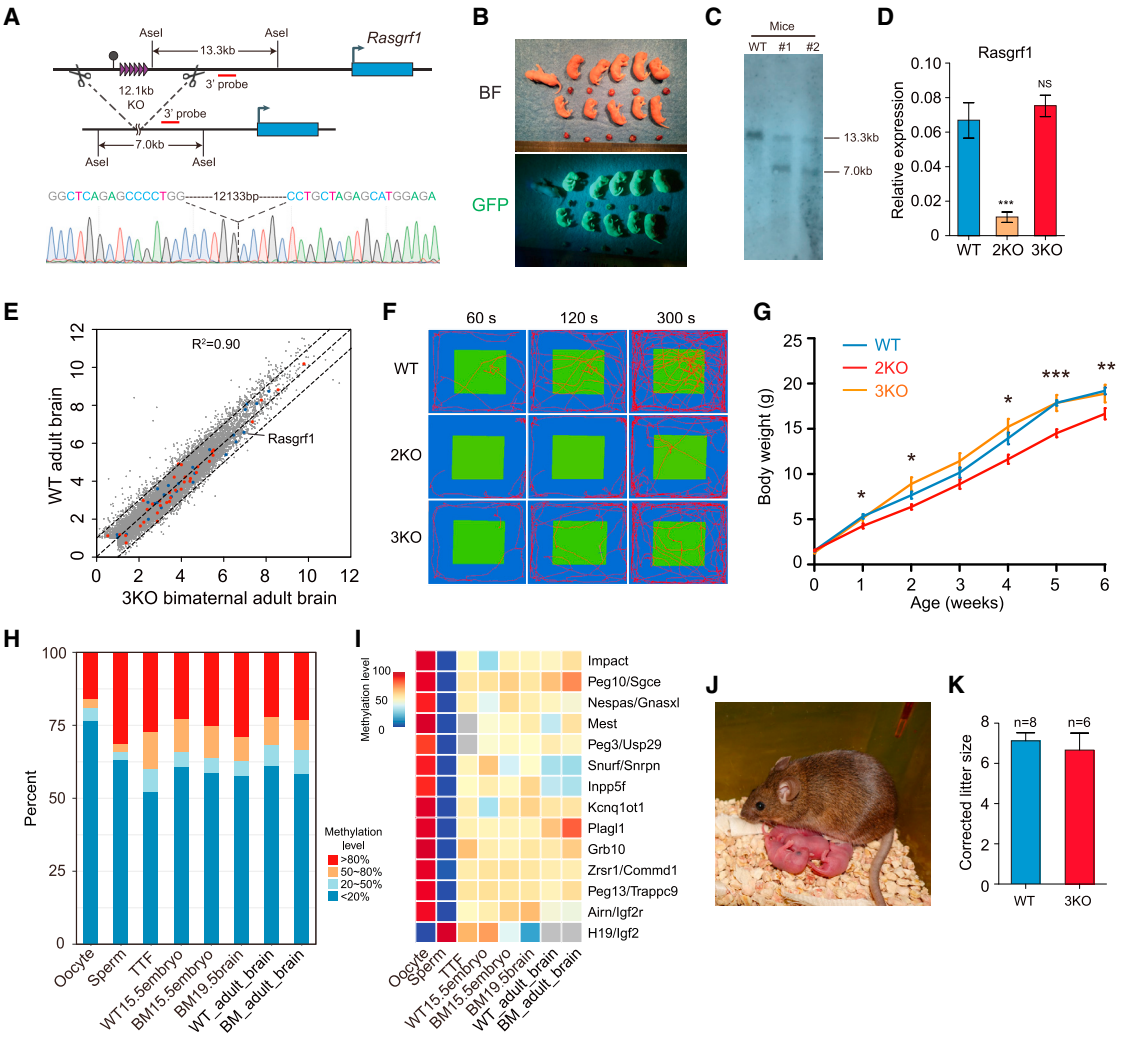

Figure 3. Generation of Normal Bimaternal Mice using 3KO-phESCs

(A) Top: scheme of 12.1-kb Rasgrf1 imprinted region deletion and Southern blot strategy. Bottom: Sanger sequencing result of Rasgrf1 imprinted region deletion in 3KO-phESCs.

(B) Full-term 3KO-bimaternal mice and placentae. A mouse without fluorescence was the control.

(C) The Southern blot analysis of Rasgrf1 imprinted region deletion in 3KO-bimaternal mice. The genomic DNA was digested with AseI.

(D) qPCR analysis of *Rasgrf1* in WT and bimaternal pup brains.

(E) Scatterplot comparison of 3KO-bimaternal and WT adult brain transcriptomes. Dashed lines, 2-fold differences.

(F) Activity traces in the open field assay show the hesitancy to enter the anxiety-provoking central areas of 2KO-bimaternal mice compared with 3KO-bimaternal and WT mice.

(G) Growth curve of female WT (n = 12), 2KO-bimaternal mice (n = 8), and 3KO-bimaternal mice (n = 12). The statistical analysis is based on body weight comparison between the WT and 2KO-bimaternal mice. The body weight of 3KO-bimaternal mice had no significant difference compared with the WT mice.

(H) Distribution of DNA methylation levels in oocytes, sperm, TTFs, WT15.5embryo (E15.5 WT embryo), BM15.5embryo (E15.5 3KO-bimaternal embryo), BM19.5brain (E19.5 3KO-bimaternal embryo brain), WT_adult_brain (adult WT mouse brain), and BM_adult_brain (adult 3KO-bimaternal mouse brain).

(I) Heatmap of imprinted region methylation in all related samples. Gray squares indicate a lack of valid reads.

(J) An adult 3KO-bimaternal mouse and its offspring.

(K) The corrected litter size of the bimaternal mouse (6.7 ± 0.84, n = 6) was comparable with the WT (7.1 ± 0.40, n = 8).

For all graphs, data are presented as mean ± SEM. *p < 0.05, **p < 0.01, ***p < 0.001. See also Figure S2.

sizes of WT females (n = 8). The corrected litter size of 3KO-bimaternal mice was calculated as 6.7 ± 0.84, comparable with the WT females (7.1 ± 0.40), indicating normal fertility (Figures 3J and 3K). These results demonstrated that all detected bimaternal reproduction barriers were crossed with the described system.

Early- and Late-Passage phESCs Are Equally Efficient in Producing Bimaternal Mice

To exclude that the phenotypic improvements of the bimaternal mice were caused by different passages between 3KO-phESCs (passage > 27) and 2KO-phESCs (IG and H19-KO, approximately passage 40) (Li et al., 2016), we derived early-passage

Table 1. Development of Uniparental Mice

Method	Cell Line	No. of Passages*	No. of Transferred Embryos	No. of Implantation Site (% ET)	No. of Embryos Arrested 10.5–17.5 (% ET)	No. of Full-Term Pups (% ET)	Pup Phenotypes (% FT)				No. of Surviving Pups (% ET)
							UE	LT	LG	DR	
Oocyte injection	round spermatid		166	–	–	25 (15.1 ± 1.0)	0	0	0	0	24 (14.5 ± 1.3)
	phESC-1KO-1	P22–P28	275	34 (12.4)	2 (0.7)	7 (2.6 ± 0.6)[a]	0	0	0	4 (100)	0[a]
	phESC-1KO-2	P21–P27	211	18 (12.9)	1 (0.7)	3 (1.1 ± 1.0)[a]	0	0	0	3 (100)	0[a]
	phESC-2KO-1	P21–P26	170	42 (23.3)	0	15 (8.5 ± 2.3)[b]	0	0	0	1 (6.7)	10 (5.0 ± 3.1)[b]
	phESC-2KO-2	P20–P26	111	19 (17.1)	1 (0.9)	10 (8.9 ± 2.5)[b]	0	0	0	1 (10)	7 (6.3 ± 1.6)[a]
	phESC-3KO-1	P27–P33	111	12 (16.9)	0	16 (14.2 ± 2.3)[c]	0	0	0	0	15 (13.4 ± 1.2)[c]
	phESC-3KO-2	P27–P35	99	19 (26.4)	0	13 (13.3 ± 2.5)[c]	0	0	0	0	12 (12.3 ± 1.9)[c]
Tetraploid complementation**	C57 ESC1-1	P16–P22	112	62	13 (11.6 ± 0.8)	4 (4.4 ± 1.2)	0	0	0	0	3 (75)
	adESC-6KO-1	P35–P39	198	120	19 (9.5 ± 1.6)[f]	3 (1.6 ± 0.4)[e]	2 (66.7)	3 (100)	2 (66)	3 (100)	0
	adESC-6KO-2	P35–P42	361	205	18 (5.3 ± 1.5)[d]	5 (1.3 ± 0.4)[e]	3 (60)	5 (100)	2 (40)	5 (100)	0
	adESC-6KO-3	P35–P45	464	302	42 (8.1 ± 2.2)[f]	4 (0.9 ± 0.3)[d]	3 (75)	4 (100)	2 (50)	4 (100)	0
	adESC-7KO-1	P43–P47	141	98	14 (10.0 ± 0.5)[e]	4 (2.8 ± 0.4)[f]	1 (25)	2 (50)	1 (25)	2 (50)	0
	adESC-7KO-2	P44–P48	129	92	9 (7.2 ± 1.3)[d]	4 (3.0 ± 0.7)[f]	1 (25)	1 (25)	1 (25)	3 (75)	0
	adESC-7KO-3	P46–P49	207	123	17 (8.5 ± 1.7)[e]	4 (1.9 ± 0.3)[e]	1 (25)	1 (25)	0	2 (50)	2 (50)***

ET, transferred embryo; FT, full term; UE, unclosed eyelid; LT, long tongue; LG, leaky gut; DR, depressed respiration. *The passage of adESCs was calculated from the establishment of ahESCs.
**The sex chromosome constitution of ESCs used for tetraploid complementation was XY. ***Dead after 48 hr.
[a]phESCs versus round spermatid ($p < 0.01$).
[b]phESCs versus round spermatid ($0.01 < p < 0.05$).
[c]phESCs versus round spermatid ($p > 0.05$).
[d]ahESCs versus C57ESC-1-1 ($p < 0.01$).
[e]ahESCs versus C57ESC-1-1 ($0.01 < p < 0.05$).
[f]ahESCs versus C57ESC-1-1 ($p > 0.05$).

2KO-phESCs (IG and H19-KO) and 1KO-phESCs (IG-KO) by CRISPR-Cas9 to reconstruct bimaternal embryos with MII oocytes. Consistent with our previous findings, the survival of bimaternal mice required deletion of both regions (Table 1). Specifically, early-passage 1KO-phESCs (passages 21∼28) and 2KO-phESCs (passages 20∼26) produced 10 (∼2.1%) and 25 (∼8.9%) full-term mice (referred as 1KO- and 2KO-bimaternal mice) from 486 and 281 transferred embryos, respectively (Table 1), comparable with our previous findings with late-passage 1KO- and 2KO-phESCs (Li et al., 2016). All 1KO-bimaternal pups died after birth with severe retardation (Table 1; Figure S2Q). The body and placenta weights were recovered in 2KO-bimaternal pups, accompanied by restoration of *Igf2* expression (Figures S2R–S2T). Additionally, the surviving 2KO-bimaternal mice exhibited ∼20% postnatal growth retardation compared with the WT (Figure 3G). These results showed that early-passage (passages 20∼26) and late-passage (approximately passage 40) phESCs were equal in producing bimaternal mice and proved that PGC-like imprint-free status was achieved in early-passage phESCs, consistent with the DNA methylation analyses (Figures 1D and 1E).

Generation of Live Bipaternal Mice with Hypomethylated ahESCs and Imprinted Region Deletions

The retardation of mouse embryos with two male pronuclei occurred much earlier than in female counterparts (Barton et al., 1984). To cross the bipaternal reproduction barriers with PGC-like ahESCs, we first chose 6 imprinted regions that have shown important parent-of-origin effects on embryonic lethality, fetal or placenta growth, and severe uniparental disomy phenotypes for deletion in *Gfp*-labeled ahESCs with more than 30 passages (referred to as 6KO-ahESC) (Figure S3; Table S2; Arnaud et al., 2003; Barlow et al., 1991; Birger et al., 1999; Dubose et al., 2011; Fitzpatrick et al., 2002; Kim et al., 2012; Weinstein et al., 2004). The imprinted regions chosen for deletion included Nespas (regulating *Nesp* and *Nespas*), Grb10 (regulating *Cobl* and *Grb10*), Igf2r (regulating *Airn* and *Igf2r*), Snrpn (regulating *Snurf* and *Snrpn*), Kcnq1 (regulating *Cdkn1c* and *Kcnq1*), and Peg3 (regulating *Usp29* and *Peg3*) (Figure S3). We then constructed 1,144 bipaternal embryos through co-injection of a 6KO-ahESC and a sperm into an enucleated oocyte (Figure S4A). However, the embryos were restricted to E8.5 after transplantation into pseudopregnant recipient mice, and none of the placentae could develop beyond E10.5 (Figure S4B). As an alternative strategy, we derived androgenetic diploid ESCs from androgenetic diploid embryos by co-injection of 6KO-ahESC and an *Rfp*-labeled sperm (referred to as 6KO-adESCs) and attempted to produce bipaternal mice by tetraploid complementation (Figures 4A and S4C). The sex chromosome constitution of 6 derived adESC lines was analyzed with PCR (XY:XX:XO = 4:2:0) (Figure S4D). The 6KO-adESCs expressed both GFP and red fluorescent protein (RFP) as well as the pluripotency markers OCT4, NANOG, and SSEA-1 (Figures S4E and S4F). They were able to form teratomas containing tissue derivatives of all three germ layers after subcutaneous injection in SCID mice and also generated adult chimeras after blastocyst injection (Figures S4G and S4H).

We injected the 6KO-adESCs into 1,023 tetraploid embryos (Figure 4A). Impressively, 12 (∼1.2%) live full-term bipaternal pups (referred to as 6KO-bipaternal mice) were produced (Table 1). However, they exhibited severe overgrowth and edema, with body weights (2.45 ± 0.09 g, n = 12) over 2 times those of the WT (1.12 ± 0.03 g, n = 10), and died shortly after birth with suckling and breathing deficiencies (Figure 4B; Video S1). The 6KO-bipaternal fetuses recovered at E15.5 had no swelling phenotypes, suggesting that the edema deficiency occurred in late embryonic stages (Figure 4C). Full-term bipaternal mice also exhibited evidence of increased inner pressure, including unclosed eyelids, leaky guts, and longer tongues (Figures 4D and 4E; Table 1).

Ameliorating the Defects of Bipaternal Mice with Gnas Imprinted Region Deletion

We found that the Gnas imprinted region was hypomethylated in 6KO-bipaternal mice and that the expression level of *Gnas* was significantly lower in 6KO-bipaternal mice than in WT mice (Figures 4F and 4G). The Gnas imprinted region was responsible for regulating the expression of *Gnas* and located within the same locus of Nespas, one of the six deleted regions in the bipaternal mice (Weinstein et al., 2004). We next deleted exon1A in the Gnas imprinted region in 6KO-ahESCs and generated 7KO-adESCs as well (Figures 5A and S4I). The sex chromosome constitution of 6 derived adESC lines was analyzed with PCR (XY:XX:XO = 4:2:0) (Figure S4D). After injection in 477 tetraploid blastocysts followed by transplantation into the surrogate mothers, the 7KO-adESCs produced 12 (∼2.5%) bipaternal mice (referred as 7KO-bipaternal mice) (Figures 5B and 5C; Table 1). Notably, the defective phenotypes were largely ameliorated in 7KO-bipaternal mice (Figure 5B). Both the body (1.67 ± 0.10 g, n = 10) and placental weights (0.22 ± 0.02 g, n = 10) were significantly reduced (Figures 5D and 5E and S4J). Furthermore, all symptoms of aberrant inner pressure were relieved in the 7KO-bipaternal mice (Table 1). Particularly, 2 of the pups without edema survived more than 48 hr (Table 1; Video S2). However, both of them failed to survive to adulthood. The sex chromosome constitution of 8 derived bipaternal mice was analyzed with PCR (XY:XO = 8:0) (Figure S5A). To ascertain the cause of death, we performed computed tomography (CT) skeletal scanning and MRI on whole-body sections of the pups. The skeletons of the bipaternal pups showed no obvious defects (Figure S5B). Compared with 6KO-bipaternal pups, macroglossia and hepatomegaly were reduced in the 7KO-bipaternal pups, but the latter was still increased compared with WT pups (Figures 5F and S5C). The RRBS analysis showed that the global methylation level of bipaternal embryos was comparable with the WT (Figure 5G), but many of the imprinted regions of the bipaternal embryo were hypomethylated (Figure 5H), proving the absence of maternal inherited imprints. Transcriptome analyses showed that most imprinted genes, including *Gnas*, were regularly expressed in 7KO-bipaternal mice. However, several imprinted genes, such as *Cdkn1c*, *Sgce*, *Plagl1*, *Zim1*, *Calcr*, and *Asb4*, were still differentially expressed (Figure 5I). Collectively, we demonstrated that the bipaternal reproduction barriers in mammals could also be crossed.

DISCUSSION

The production of bimaternal and bipaternal mice showed that uniparental reproduction barriers were crossed using a

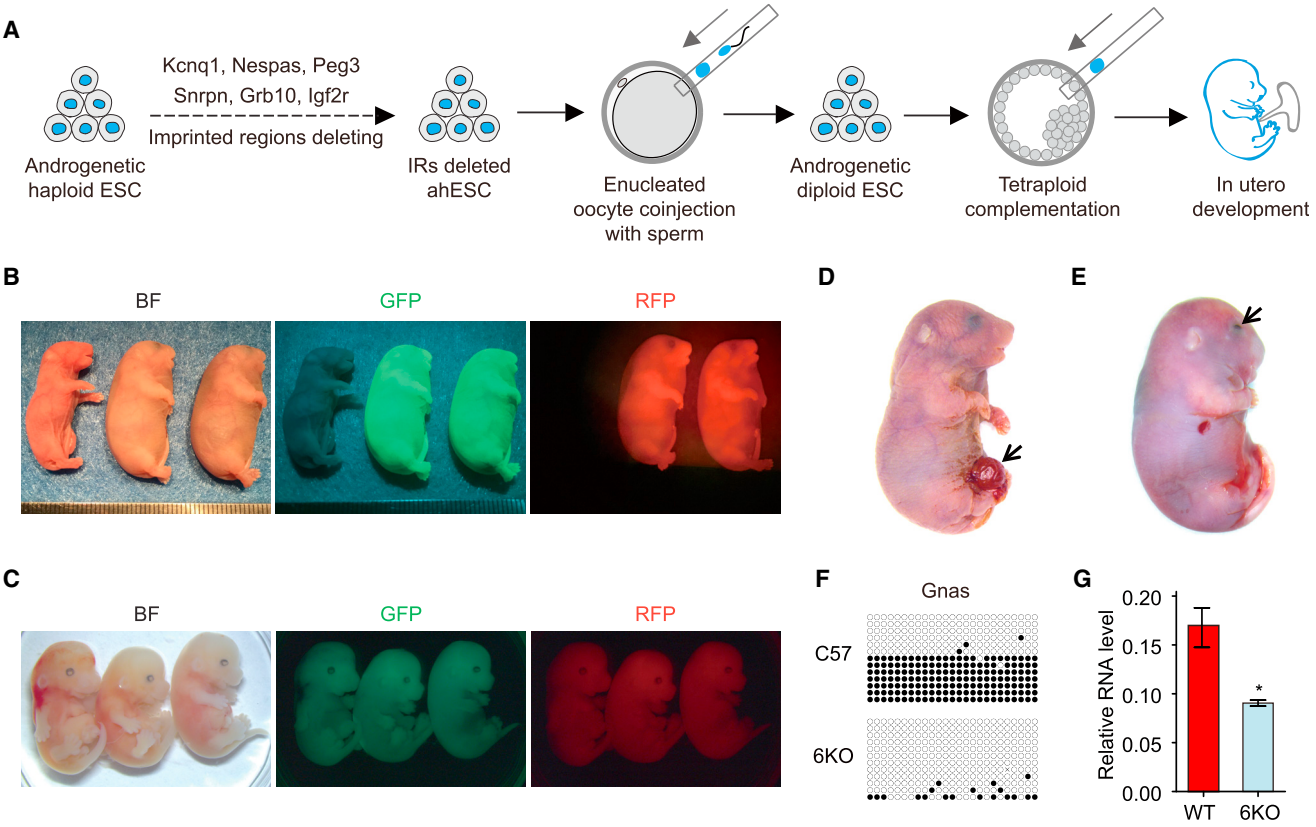

Figure 4. Production of Live Bipaternal Mice using 6KO-adESCs

(A) Schematic of the generation of bipaternal mice by tetraploid complementation of imprinted region-deleted adESCs.

(B) Live bipaternal mice produced from 6KO-adESCs by tetraploid complementation. The left mouse without fluorescence was the control.

(C) Bipaternal 6KO-bipaternal fetus recovered on E15.5.

(D) Leaky gut phenotype of 6KO-bipaternal mice.

(E) Unclosed eyelid phenotype of 6KO-bipaternal mice.

(F) DNA methylation analysis of Gnas exon1A in WT and 6KO-bipaternal pups by bisulfite sequencing.

(G) qPCR analysis of expression levels of *Gnas* in the adipose tissue of WT and 6KO-bipaternal pups.

For all graphs, data are presented as mean ± SEM. *p < 0.05. See also Figures S3 and S4.

PGC-like hypomethylation status in haploid ESCs with specific imprinted region deletions (Figure 5J). In the bipaternal embryos, the sperm genome contained intact paternal imprints. For the bimaternal embryos, the MII oocytes had entire maternal imprints. The uniparental disomies of 7 chromosomes or 11 segments can cause severe defects or embryonic lethality (Berger and Epstein, 1989; Cattanach, 1986; Cattanach et al., 1996; Cattanach and Jones, 1994; Cattanach and Kirk, 1985; Cattanach and Rasberry, 1993; Johnson, 1974; Searle and Beechey, 1978, 1990). However, bimaternal mice produced with 3 imprinted region modifications did not show the growth retardation or other abnormalities observed in the 2KO-bimaternal mice. Thus, the PGC-like imprint-free status in phESCs had compromised additional uniparental deficiencies in the reconstructed embryos. Similarly, the PGC-like status in ahESCs was also supportive on crossing the bipaternal reproduction barrier.

Using immature oocytes with the H19 region deletion, Kono et al. (2004) produced the first surviving H19-KO bimaternal mice. Subsequently, they found that an additional deletion of the Dlk1-Gtl2 region could increase efficiency (Kawahara et al., 2007b). However, it is worth noting that the Dlk1-Gtl2 imprint on the paternal genome is indispensable for normal embryonic development (da Rocha et al., 2008; Georgiades et al., 2000). Thus, at least part of the immature oocytes maintained (or regained) imprint at the Dlk1-Gtl2 region or live H19-KO bimaternal mice could not be born. In fact, Kono et al. (2004) reported abnormal methylation levels of Dlk1-Gtl2 in post-mortem H19-KO bimaternal pups, which led them to deletion of IG and extended the development of nonviable bimaternal embryos (Kawahara et al., 2007a, 2007b). In contrast, deletion of both the H19 and IG regions was required to produce surviving bimaternal mice in our study (Table 1; Li et al., 2016). Additionally, bisulfite sequencing and RRBS analyses showed complete erasure of H19 and Dlk1-Gtl2 imprints in early-passage phESCs (Figures 1D and 1E). The results suggested a more homogeneous imprint-free status in early-passage phESCs than in immature oocytes, the descendants of PGCs.

Studies of nuclear transplantation of diploid imprint-free PGCs have shown that the reconstituted oocytes developed to day 9.5 of gestation, with severely retarded embryos and abnormal

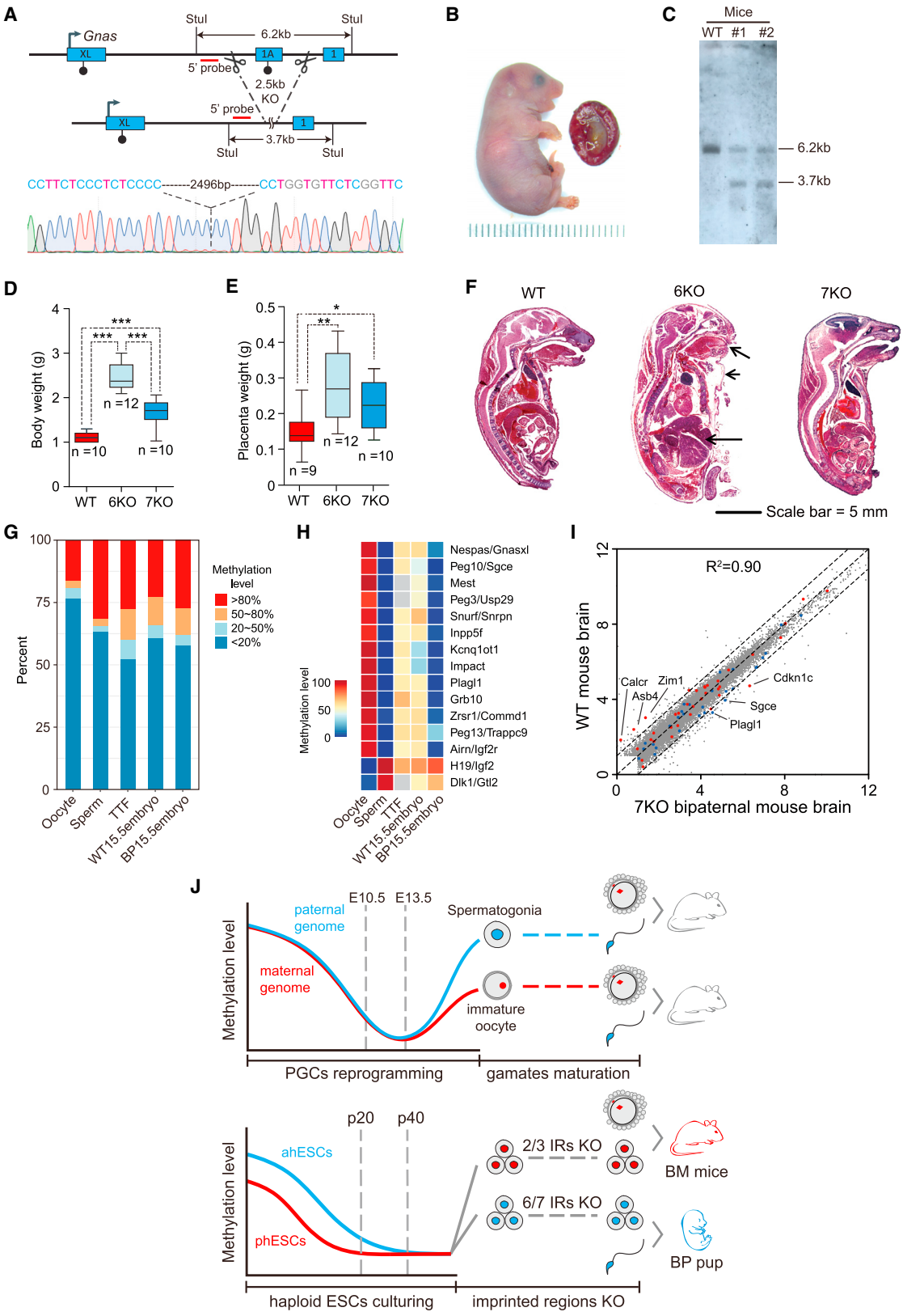

(legend on next page)

placentae (Kato et al., 1999). We also reported that MII oocyte injection of imprint-free phESCs without imprinted region deletion could not develop beyond E13.5 (Li et al., 2016). These results demonstrate that the PGC-like state alone is not sufficient to cross the uniparental development barrier without proper modifications.

The molecular mechanisms controlling imprinting at different regions are quite complex and have not been fully elucidated. For instance, activation of *Rasgrf1* gene expression has been suggested to be regulated by the change of CTCF-dependent chromatin interaction within the locus through methylation of the imprinted region (Yoon et al., 2005), similar to another CTCF regulation-dependent imprinting gene, *H19* (Hark et al., 2000; Kurukuti et al., 2006). But this hypothesis for Rasgrf1 imprinting lacks functional evidence. In this study we showed that *Rasgrf1* expression could be activated by Rasgrf1 imprinted region deletion in 3KO-bimaternal mice. This is *in vivo* evidence that supports the CTCF-dependent enhancer-blocking hypothesis of Rasgrf1 (Yoon et al., 2005). Interestingly, the recovery of *Th* and *Xlr3b* in 3KO-bimaternal mice also implied a possible regulating role of *Rasgrf1* in the brain. However, several imprinted regions have been reported to function through CTCF-dependent enhancer blocking to date (Phillips and Corces, 2009). On the other hand, new mechanisms, such as DNA methylation-independent placenta imprinting, are also emerging (Inoue et al., 2017).

Phenotype analyses of uniparental mice revealed that two paternal genomes increased (Figures 5D–5F) whereas two maternal genomes decreased organ and body size (Figures S2Q and S2S), which supports the conflict theory, a hypothesis that assumes a resource acquisition competition relationship between mother and offspring in which the paternal inherited genome promoted but the maternal inherited genome hindered the growth of offspring (Wilkins and Haig, 2003). In addition, the distinct results of co-injecting ahESC with sperm (Figures S4A and S4B) and tetraploid complementation of 6KO-adESCs (Figures 4A and 4B) imply a crucial role of H3K27me3-dependent placenta imprinting in embryo development (Inoue et al., 2017; Lewis et al., 2004).

Global demethylation was previously found in mouse diploid ESCs under serum and leukemia inhibitory factor (LIF) (Zvetkova et al., 2005) or 2i and LIF culture (Choi et al., 2017; Ficz et al., 2013; Habibi et al., 2013; Yagi et al., 2017). We also confirmed DNA hypomethylation in diploid ESCs (Figures 1B, 1C, S1A, and S1B). Thus, DNA hypomethylation and the epigenomic similarity to PGCs is not a haploid-specific phenomenon. Notably, we found that both ahESCs and phESCs experienced demethylating processes with different dynamics. Although ahESCs still maintained global methylation and imprints at passage 20, phESCs exhibited hypomethylation and loss of imprints (Figures 1B and 1D). The bisulfite sequencing results also confirmed different loss-of-imprint speeds in phESCs and ahESCs (Figures 1E, S1D, and S1E). These findings suggested allele-related factors affecting ESC demethylation, which remains to be explored. Taking into consideration the successful generation of haploid ESCs in multiple species (Leeb and Wutz, 2011; Li et al., 2012, 2014; Sagi et al., 2016; Yang et al., 2012, 2013), the results of the present study may also reveal many aspects of mammal reproduction.

STAR★METHODS

Detailed methods are provided in the online version of this paper and include the following:

- KEY RESOURCES TABLE
- CONTACT FOR REAGENT AND RESOURCE SHARING
- EXPERIMENTAL MODEL AND SUBJECT DETAILS
  - Animals care and use
  - Oocyte collection
  - Derivation and culture of ES cell and haploid ES cell lines
  - CRISPR/Cas mediated imprinted region deletion
  - Southern blot
  - Immunofluorescence staining
  - Teratoma formation and histological analysis
  - Diploid blastocyst injection
  - Intracytoplasmic injection of phESCs and round spermatid
  - Coinjection of androgenetic haploid ESCs and sperm
  - Establishment of diploid androgenetic ES cells
  - Tetraploid embryo complementation of ESCs and diploid androgenetic ESCs
  - RNA-seq library preparation and data analysis
  - RRBS library preparation and data analysis
  - Open-field test

Figure 5. Ameliorating Bipaternal Mouse Defects with Gnas Region Deletion

(A) Top: schematic of 2.5-kb Gnas imprinted region deletion and Southern blot strategy. Bottom: Sanger sequencing result of Gnas imprinted region deletion in 7KO-ahESCs.

(B) Surviving bipaternal pups produced from 7KO-adESCs by tetraploid complementation.

(C) Southern blot analysis of Gnas imprinted region deletion in 7KO-bipaternal mice. The genomic DNA was digested with StuI.

(D) The body weights of WT and 7KO-bipaternal pups.

(E) Placental weights of pups derived from tetraploid complementation of WT-ESCs, tetraploid complementation of 6KO-adESCs, and tetraploid complementation of 7KO-adESCs.

(F) Whole-body section showing edema (arrowhead), enlarged tongue (short arrow), and liver (long arrow) in 6KO-bipaternal pups (n = 2) compared with 7KO bipaternal pups (n = 2) and WT pups (n = 2).

(G) Distribution of DNA methylation levels in oocytes, sperm, TTFs, WT15.5embryo (E15.5 WT embryo), and BP15.5embryo (E15.5 7KO-bipaternal embryo).

(H) Heatmap of imprinted region methylation in related samples. Gray squares indicate a lack of valid reads.

(I) Scatterplot comparison of 7KO-bipaternal and WT pup brain transcriptomes. Dashed lines depicted 2-fold changes. R^2 was determined by Pearson's correlation.

(J) Similar to reprogramming PGCs, the haploid ESCs genomes underwent demethylation and loss of imprints. The PGC-like status with specific imprinted region deletions could cross uniparental reproduction barriers. IR, imprinted region.

For all graphs, data are presented as mean ± SEM. *p < 0.05, **p < 0.01, ***p < 0.001. N.S., not significant.See also Figures S4 and S5.

SUPPLEMENTAL INFORMATION

Supplemental Information includes five figures, three tables, and two videos and can be found with this article online at https://doi.org/10.1016/j.stem.2018.09.004.

ACKNOWLEDGMENTS

This study was supported by the Strategic Priority Research Program of the Chinese Academy of Sciences (XDA16000000); the National Basic Research Program of China (2014CB964800); the National Key Research and Development Program (2017YFA0103803); the National High Technology R&D Program (2015AA020307); the National Natural Science Foundation of China (31621004, 31422038, and 31471395); the Key Research Projects of the Frontier Science of the Chinese Academy of Sciences (QYZDY-SSW-SMC002 and QYZDB-SSW-SMC022); the National Postdoctoral Program for Innovative Talents (BX201600161 and BX201700243); and the Ferring Institute of Reproductive Medicine, a strategic collaborative research program of Ferring Pharmaceuticals and Chinese Academy of Sciences (FIRMD180304). We thank Shi-Wen Li, Xi-Li Zhu, and Qing Meng for help with fluorescence-activated cell sorting and confocal laser-scanning microscopy.

AUTHOR CONTRIBUTIONS

B.-Y.H., Q.Z., and W.L. conceived this project and supervised all experiments and data analyses. B.-Y.H., Q.Z., W.L., and Z.-K.L. analyzed the data and wrote the manuscript. Z.-K.L., L.-Y.W., L.-B.W., G.-H.F., and X.-W.Y. performed the experiments and analyzed the data. G.-H.F. performed the bioinformatics analysis. C.L., K.X., Y.-H.L., H.-F.W., Y.Z., Y.-F.L., and X.L. performed experiments.

DECLARATION OF INTERESTS

The authors declare no competing interests.

Received: March 25, 2018
Revised: July 16, 2018
Accepted: September 5, 2018
Published: October 11, 2018

REFERENCES

Arnaud, P., Monk, D., Hitchins, M., Gordon, E., Dean, W., Beechey, C.V., Peters, J., Craigen, W., Preece, M., Stanier, P., et al. (2003). Conserved methylation imprints in the human and mouse GRB10 genes with divergent allelic expression suggests differential reading of the same mark. Hum. Mol. Genet. *12*, 1005–1019.

Barlow, D.P., Stöger, R., Herrmann, B.G., Saito, K., and Schweifer, N. (1991). The mouse insulin-like growth factor type-2 receptor is imprinted and closely linked to the Tme locus. Nature *349*, 84–87.

Bartolomei, M.S., and Ferguson-Smith, A.C. (2011). Mammalian genomic imprinting. Cold Spring Harb. Perspect. Biol *3*, a002592.

Bartolomei, M.S., Zemel, S., and Tilghman, S.M. (1991). Parental imprinting of the mouse H19 gene. Nature *351*, 153–155.

Barton, S.C., Surani, M.A.H., and Norris, M.L. (1984). Role of paternal and maternal genomes in mouse development. Nature *311*, 374–376.

Berger, C.N., and Epstein, C.J. (1989). Genomic imprinting: normal complementation of murine chromosome 16. Genet. Res. *54*, 227–230.

Birger, Y., Shemer, R., Perk, J., and Razin, A. (1999). The imprinting box of the mouse Igf2r gene. Nature *397*, 84–88.

Cattanach, B.M. (1986). Parental origin effects in mice. J. Embryol. Exp. Morphol. *97* (*Suppl*), 137–150.

Cattanach, B.M., and Jones, J. (1994). Genetic imprinting in the mouse: implications for gene regulation. J. Inherit. Metab. Dis. *17*, 403–420.

Cattanach, B.M., and Kirk, M. (1985). Differential activity of maternally and paternally derived chromosome regions in mice. Nature *315*, 496–498.

Cattanach, B.M., and Rasberry, C. (1993). Evidence of imprinting involving the distal region of Chr 12. Mouse Genome *91*, 858–863.

Cattanach, B.M., Beechey, C.V., Rasberry, C., Jones, J., and Papworth, D. (1996). Time of initiation and site of action of the mouse chromosome 11 imprinting effects. Genet. Res. *68*, 35–44.

Choi, J., Huebner, A.J., Clement, K., Walsh, R.M., Savol, A., Lin, K., Gu, H., Di Stefano, B., Brumbaugh, J., Kim, S.Y., et al. (2017). Prolonged Mek1/2 suppression impairs the developmental potential of embryonic stem cells. Nature *548*, 219–223.

Constância, M., Kelsey, G., and Reik, W. (2004). Resourceful imprinting. Nature *432*, 53–57.

Corley-Smith, G.E., Lim, C.J., and Brandhorst, B.P. (1996). Production of androgenetic zebrafish (Danio rerio). Genetics *142*, 1265–1276.

da Rocha, S.T., Edwards, C.A., Ito, M., Ogata, T., and Ferguson-Smith, A.C. (2008). Genomic imprinting at the mammalian Dlk1-Dio3 domain. Trends Genet. *24*, 306–316.

Dai, X., Hao, J., and Zhou, Q. (2009). A modified culture method significantly improves the development of mouse somatic cell nuclear transfer embryos. Reproduction *138*, 301–308.

Davies, W., Isles, A., Smith, R., Karunadasa, D., Burrmann, D., Humby, T., Ojarikre, O., Biggin, C., Skuse, D., Burgoyne, P., and Wilkinson, L. (2005). Xlr3b is a new imprinted candidate for X-linked parent-of-origin effects on cognitive function in mice. Nat. Genet. *37*, 625–629.

Drake, N.M., DeVito, L.M., Cleland, T.A., and Soloway, P.D. (2011). Imprinted Rasgrf1 expression in neonatal mice affects olfactory learning and memory. Genes Brain Behav. *10*, 392–403.

Dubose, A.J., Smith, E.Y., Yang, T.P., Johnstone, K.A., and Resnick, J.L. (2011). A new deletion refines the boundaries of the murine Prader-Willi syndrome imprinting center. Hum. Mol. Genet. *20*, 3461–3466.

Ferguson-Smith, A.C., Cattanach, B.M., Barton, S.C., Beechey, C.V., and Surani, M.A. (1991). Embryological and molecular investigations of parental imprinting on mouse chromosome 7. Nature *351*, 667–670.

Ficz, G., Hore, T.A., Santos, F., Lee, H.J., Dean, W., Arand, J., Krueger, F., Oxley, D., Paul, Y.L., Walter, J., et al. (2013). FGF signaling inhibition in ESCs drives rapid genome-wide demethylation to the epigenetic ground state of pluripotency. Cell Stem Cell *13*, 351–359.

Fitzpatrick, G.V., Soloway, P.D., and Higgins, M.J. (2002). Regional loss of imprinting and growth deficiency in mice with a targeted deletion of KvDMR1. Nat. Genet. *32*, 426–431.

Georgiades, P., Watkins, M., Surani, M.A., and Ferguson-Smith, A.C. (2000). Parental origin-specific developmental defects in mice with uniparental disomy for chromosome 12. Development *127*, 4719–4728.

Gu, H., Smith, Z.D., Bock, C., Boyle, P., Gnirke, A., and Meissner, A. (2011). Preparation of reduced representation bisulfite sequencing libraries for genome-scale DNA methylation profiling. Nat. Protoc. *6*, 468–481.

Guo, H., Hu, B., Yan, L., Yong, J., Wu, Y., Gao, Y., Guo, F., Hou, Y., Fan, X., Dong, J., et al. (2017). DNA methylation and chromatin accessibility profiling of mouse and human fetal germ cells. Cell Res. *27*, 165–183.

Habibi, E., Brinkman, A.B., Arand, J., Kroeze, L.I., Kerstens, H.H.D., Matarese, F., Lepikhov, K., Gut, M., Brun-Heath, I., Hubner, N.C., et al. (2013). Whole-genome bisulfite sequencing of two distinct interconvertible DNA methylomes of mouse embryonic stem cells. Cell Stem Cell *13*, 360–369.

Hark, A.T., Schoenherr, C.J., Katz, D.J., Ingram, R.S., Levorse, J.M., and Tilghman, S.M. (2000). CTCF mediates methylation-sensitive enhancer-blocking activity at the H19/Igf2 locus. Nature *405*, 486–489.

Hiura, H., Obata, Y., Komiyama, J., Shirai, M., and Kono, T. (2006). Oocyte growth-dependent progression of maternal imprinting in mice. Genes Cells *11*, 353–361.

Inoue, A., Jiang, L., Lu, F., Suzuki, T., and Zhang, Y. (2017). Maternal H3K27me3 controls DNA methylation-independent imprinting. Nature *547*, 419–424.

Johnson, D.R. (1974). Hairpin-tail: a case of post-reductional gene action in the mouse egg. Genetics *76*, 795–805.

Kato, Y., Rideout, W.M., 3rd, Hilton, K., Barton, S.C., Tsunoda, Y., and Surani, M.A. (1999). Developmental potential of mouse primordial germ cells. Development *126*, 1823–1832.

Kawahara, M., Wu, Q., Ferguson-Smith, A.C., and Kono, T. (2007a). Appropriate expression of imprinted genes on mouse chromosome 12 extends development of bi-maternal embryos to term. FEBS Lett. *581*, 5178–5184.

Kawahara, M., Wu, Q., Takahashi, N., Morita, S., Yamada, K., Ito, M., Ferguson-Smith, A.C., and Kono, T. (2007b). High-frequency generation of viable mice from engineered bi-maternal embryos. Nat. Biotechnol. *25*, 1045–1050.

Kim, J., Ekram, M.B., Kim, H., Faisal, M., Frey, W.D., Huang, J.M., Tran, K., Kim, M.M., and Yu, S. (2012). Imprinting control region (ICR) of the Peg3 domain. Hum. Mol. Genet. *21*, 2677–2687.

Kobayashi, H., Sakurai, T., Miura, F., Imai, M., Mochiduki, K., Yanagisawa, E., Sakashita, A., Wakai, T., Suzuki, Y., Ito, T., et al. (2013). High-resolution DNA methylome analysis of primordial germ cells identifies gender-specific reprogramming in mice. Genome Res. *23*, 616–627.

Kono, T., Obata, Y., Wu, Q., Niwa, K., Ono, Y., Yamamoto, Y., Park, E.S., Seo, J.S., and Ogawa, H. (2004). Birth of parthenogenetic mice that can develop to adulthood. Nature *428*, 860–864.

Kurukuti, S., Tiwari, V.K., Tavoosidana, G., Pugacheva, E., Murrell, A., Zhao, Z., Lobanenkov, V., Reik, W., and Ohlsson, R. (2006). CTCF binding at the H19 imprinting control region mediates maternally inherited higher-order chromatin conformation to restrict enhancer access to Igf2. Proc. Natl. Acad. Sci. USA *103*, 10684–10689.

Lane, N., Dean, W., Erhardt, S., Hajkova, P., Surani, A., Walter, J., and Reik, W. (2003). Resistance of IAPs to methylation reprogramming may provide a mechanism for epigenetic inheritance in the mouse. Genesis *35*, 88–93.

Leeb, M., and Wutz, A. (2011). Derivation of haploid embryonic stem cells from mouse embryos. Nature *479*, 131–134.

Lewis, A., Mitsuya, K., Umlauf, D., Smith, P., Dean, W., Walter, J., Higgins, M., Feil, R., and Reik, W. (2004). Imprinting on distal chromosome 7 in the placenta involves repressive histone methylation independent of DNA methylation. Nat. Genet. *36*, 1291–1295.

Li, W., Shuai, L., Wan, H., Dong, M., Wang, M., Sang, L., Feng, C., Luo, G.Z., Li, T., Li, X., et al. (2012). Androgenetic haploid embryonic stem cells produce live transgenic mice. Nature *490*, 407–411.

Li, W., Li, X., Li, T., Jiang, M.G., Wan, H., Luo, G.Z., Feng, C., Cui, X., Teng, F., Yuan, Y., et al. (2014). Genetic modification and screening in rat using haploid embryonic stem cells. Cell Stem Cell *14*, 404–414.

Li, Z., Wan, H., Feng, G., Wang, L., He, Z., Wang, Y., Wang, X.J., Li, W., Zhou, Q., and Hu, B. (2016). Birth of fertile bimaternal offspring following intracytoplasmic injection of parthenogenetic haploid embryonic stem cells. Cell Res. *26*, 135–138.

McGrath, J., and Solter, D. (1983). Nuclear transplantation in the mouse embryo by microsurgery and cell fusion. Science *220*, 1300–1302.

McGrath, J., and Solter, D. (1984). Completion of mouse embryogenesis requires both the maternal and paternal genomes. Cell *37*, 179–183.

Neaves, W.B., and Baumann, P. (2011). Unisexual reproduction among vertebrates. Trends Genet. *27*, 81–88.

Phillips, J.E., and Corces, V.G. (2009). CTCF: master weaver of the genome. Cell *137*, 1194–1211.

Sagi, I., Chia, G., Golan-Lev, T., Peretz, M., Weissbein, U., Sui, L., Sauer, M.V., Yanuka, O., Egli, D., and Benvenisty, N. (2016). Derivation and differentiation of haploid human embryonic stem cells. Nature *532*, 107–111.

Searle, A.G., and Beechey, C.V. (1978). Complementation studies with mouse translocations. Cytogenet. Cell Genet. *20*, 282–303.

Searle, A.G., and Beechey, C.V. (1990). Genome imprinting phenomena on mouse chromosome 7. Genet. Res. *56*, 237–244.

Suh, Y., Atzmon, G., Cho, M.O., Hwang, D., Liu, B., Leahy, D.J., Barzilai, N., and Cohen, P. (2008). Functionally significant insulin-like growth factor I receptor mutations in centenarians. Proc. Natl. Acad. Sci. USA *105*, 3438–3442.

Surani, M.A.H., and Barton, S.C. (1983). Development of gynogenetic eggs in the mouse: implications for parthenogenetic embryos. Science *222*, 1034–1036.

Surani, M.A.H., Barton, S.C., and Norris, M.L. (1984). Development of reconstituted mouse eggs suggests imprinting of the genome during gametogenesis. Nature *308*, 548–550.

Trapnell, C., Williams, B.A., Pertea, G., Mortazavi, A., Kwan, G., van Baren, M.J., Salzberg, S.L., Wold, B.J., and Pachter, L. (2010). Transcript assembly and quantification by RNA-Seq reveals unannotated transcripts and isoform switching during cell differentiation. Nat. Biotechnol. *28*, 511–515.

Trapnell, C., Roberts, A., Goff, L., Pertea, G., Kim, D., Kelley, D.R., Pimentel, H., Salzberg, S.L., Rinn, J.L., and Pachter, L. (2012). Differential gene and transcript expression analysis of RNA-seq experiments with TopHat and Cufflinks. Nat. Protoc. *7*, 562–578.

Wan, H., He, Z., Dong, M., Gu, T., Luo, G.Z., Teng, F., Xia, B., Li, W., Feng, C., Li, X., et al. (2013). Parthenogenetic haploid embryonic stem cells produce fertile mice. Cell Res. *23*, 1330–1333.

Weinstein, L.S., Liu, J., Sakamoto, A., Xie, T., and Chen, M. (2004). Minireview: GNAS: normal and abnormal functions. Endocrinology *145*, 5459–5464.

Wilkins, J.F., and Haig, D. (2003). What good is genomic imprinting: the function of parent-specific gene expression. Nat. Rev. Genet. *4*, 359–368.

Yagi, M., Kishigami, S., Tanaka, A., Semi, K., Mizutani, E., Wakayama, S., Wakayama, T., Yamamoto, T., and Yamada, Y. (2017). Derivation of ground-state female ES cells maintaining gamete-derived DNA methylation. Nature *548*, 224–227.

Yang, H., Shi, L., Wang, B.A., Liang, D., Zhong, C., Liu, W., Nie, Y., Liu, J., Zhao, J., Gao, X., et al. (2012). Generation of genetically modified mice by oocyte injection of androgenetic haploid embryonic stem cells. Cell *149*, 605–617.

Yang, H., Liu, Z., Ma, Y., Zhong, C., Yin, Q., Zhou, C., Shi, L., Cai, Y., Zhao, H., Wang, H., et al. (2013). Generation of haploid embryonic stem cells from Macaca fascicularis monkey parthenotes. Cell Res. *23*, 1187–1200.

Yoon, B., Herman, H., Hu, B., Park, Y.J., Lindroth, A., Bell, A., West, A.G., Chang, Y., Stablewski, A., Piel, J.C., et al. (2005). Rasgrf1 imprinting is regulated by a CTCF-dependent methylation-sensitive enhancer blocker. Mol. Cell. Biol. *25*, 11184–11190.

Zhao, X.Y., Li, W., Lv, Z., Liu, L., Tong, M., Hai, T., Hao, J., Guo, C.L., Ma, Q.W., Wang, L., et al. (2009). iPS cells produce viable mice through tetraploid complementation. Nature *461*, 86–90.

Zhou, Q.Y., and Palmiter, R.D. (1995). Dopamine-deficient mice are severely hypoactive, adipsic, and aphagic. Cell *83*, 1197–1209.

Zvetkova, I., Apedaile, A., Ramsahoye, B., Mermoud, J.E., Crompton, L.A., John, R., Feil, R., and Brockdorff, N. (2005). Global hypomethylation of the genome in XX embryonic stem cells. Nat. Genet. *37*, 1274–1279.

STAR★METHODS

KEY RESOURCES TABLE

REAGENT or RESOURCE	SOURCE	IDENTIFIER
Antibodies		
Oct4	Santa Cruz	Cat# sc-8628; RRID: AB_653551
Nanog	Abcam	Cat# ab80892; RRID: AB_2150114
SSEA1	Millipore	Cat# MAB-4301; RRID: AB_177627
Bacterial and Virus Strains		
Trans1-T1 Competent Cell	Transgen	CD501
Chemicals, Peptides, and Recombinant Proteins		
PMSG	ProSpec	HOR-272
hCG	ProSpec	HOR-250
M2	Sigma	M7167
M16	Sigma	M7292
KSOM	Millipore	MR-020P-D
Cytochalasin B	Abcam	ab143482
CHIR99021	Stemgent	04-0004
PD0325901	Stemgent	04-0006
LIF	Millipore	ESG1107
Hoechst 33342	Invitrogen	H3570
G418	GIBCO	11811031
Puromycin	GIBCO	A1113803
Critical Commercial Assays		
Cholesterol Fluorometric Assay Kit	Cayman	10007640
Experimental Models: Cell Lines		
Mouse: haploid embryonic stem cells	This paper	N/A
Mouse: embryonic stem cells	This paper	N/A
Deposited Data		
RNA-Seq	This paper	BIG: CRA001069; GEO: GSE120039
Experimental Models: Organisms/Strains		
Mouse: B6D2F1 (C57BL/6 × DBA/2)	Beijing Vital River	Cat# 302; RRID: MGI: 5649818
Mouse: CD-1	Beijing Vital River	Cat# 201; RRID: MGI: 5659424
Mouse: 129S2/SvPasCrl	Beijing Vital River	Cat# 217; RRID: IMSR_CRL: 287
Mouse: B6.129(Cg)-Gt(ROSA) 26Sortm4$^{(ACTB-tdTomato-EGFP)}$/Nju	The Jackson Laboratory	Cat# 007676; RRID: IMSR_JAX:007676
Oligonucleotides		
PCR Primers and sgRNAs	Table S1	BGI
Recombinant DNA		
pEASY-T1	Transgen	CT101
Software and Algorithms		
TopHat2	http://ccb.jhu.edu	2.1.1
Cufflinks	http://cole-trapnell-lab.github.io/cufflinks/	2.2.1
Bismark	Babraham Bioinformatics	0.13.1
Trim Galore!	Babraham Bioinformatics	0.4.3
Plot3D	R	3.2.5
Heatmap.2	R	3.2.5
Ggplot2	R	3.2.5
GraphPad Prism	GraphPad	6
Snapgene	Snapgene	2.3.2

CONTACT FOR REAGENT AND RESOURCE SHARING

Further information and requests of reagents can be directed to and fulfilled by the Lead Contact, Qi Zhou (qzhou@ioz.ac.cn). MTAs required.

EXPERIMENTAL MODEL AND SUBJECT DETAILS

Animals care and use

Specific-pathogen-free (SPF)-grade mice were obtained from Beijing Vital River Laboratories and housed in the animal facilities of the Chinese Academy of Sciences. All the studies were carried out in accordance with the Guidelines for the Use of Animals in Research issued by the Institute of Zoology, Chinese Academy of Sciences. Female mice of B6D2F1 (C57BL/6 × DBA/2) and CD-1 backgrounds were used to provide oocytes and as pseudopregnant surrogates for micromanipulation, respectively. Male mice (B6.129(Cg)-*Gt(ROSA)26Sor*$^{tm4(ACTB-tdTomato,-EGFP)Luo}$/J) were used to provide sperm for establishment of androgenetic diploid ESCs.

Oocyte collection

Mature oocytes were collected from eight-week-old female mice that had been induced to superovulate by injection of 7.5 IU pregnant mare's serum gonadotropin (PMSG) followed by 7.5 IU human chorionic gonadotropin (hCG). Oocytes were collected from the oviduct 13-15 hours after hCG injection, and were placed in HEPES-CZB and then treated with 0.1% hyaluronidase until the cumulus cells dispersed. Derived oocytes were cultured in M16 medium (Sigma) with paraffin oil (Sigma) and stored at 37°C (5% CO2/air) (Wan et al., 2013).

Derivation and culture of ES cell and haploid ES cell lines

ESC and haploid ESC-line derivation and culture were carried out as previously described (Li et al., 2012). Briefly, ESCs were cultured in 2i medium plus 5% knockout serum replacement (GIBCO). The 2i medium consists of N2B27 medium supplemented with 3 μM GSK3β inhibitor CHIR99021 (Stemgent), 1 μM MEK inhibitor PD0325901 (Stemgent), and mouse LIF (Millipore). To enrich haploid cells, the established haploid cell lines were purified by fluorescence-activated cell sorting (FACS) after being cultured for 5–7 passages. Haploid cell lines and control diploid ESCs were incubated with Hoechst 33342 (Invitrogen) for 15 min in a water bath at 37°C, and then sorted and analyzed on a Beckman MoFlow XDP II (Beckman).

CRISPR/Cas mediated imprinted region deletion

We constructed ten pairs of sgRNAs targeting different imprinted regions (Table S2). For the deletion of imprinted regions, plasmid encoding sgRNAs and Cas9 were transfected into 10^6 haploid ESCs by neon (Invitrogen). Two days after transfection, successfully transfected ESCs were sorted based on GFP or RFP fluorescence and seeded on feeder cells at low density. 7 days after culture, single colonies were picked for PCR detection and expansion (Table S2).

Southern blot

Genomic DNA was extracted from cells or mouse tissue and digested with endonucleases (Takara) overnight at 37°C. The digested genomic fragments were separated on a 0.8% agarose gel and transferred to a positively charged nylon membrane (Roche) for hybridization. The primers for amplifying the digoxigenin-labeled probe were synthesized (Table S2). The hybridization and detection procedures were performed according to the manufacturer's instruction of PCR DIG Probe Synthesis Kit (Roche).

Immunofluorescence staining

Immunostaining was carried out as previously described (Zhao et al., 2009). In brief, samples were fixed with 4% paraformaldehyde for 30 min at room temperature and then washed twice with PBS. Non-specific sites were blocked with 400 μL of 2% bovine serum albumin (BSA) plus 0.3% Triton X-100 for 1 h at room temperature. The samples were then incubated with primary antibodies overnight at 4°C. Primary antibodies included anti-OCT4 (Santa Cruz, sc-8628), anti-SSEA1 (Millipore, MAB-4301), and anti-NANOG (Abcam, ab80892). Following incubation, samples were washed three times with PBS, incubated with a Cy3-AffiniPure secondary antibody (Jackson Immunoresearch, 711-165-152-JIR) at room temperature for 1 h, and then imaged with a LSM780 Meta confocal microscope (Zeiss).

Teratoma formation and histological analysis

ESCs were trypsinized and suspended at 1 × 10^7 per mL. One-hundred microliters of the cell suspension was injected into the subcutaneous flanks of SCID mice. Four to five weeks later, the mice were euthanized and the tumors were fixed and sliced. Sections were stained with hematoxylin and eosin.

Diploid blastocyst injection

Diploid blastocyst injection and chimera generation assay was also carried out to evaluate the pluripotency of haploid ESCs. Superovulated female CD-1 mice (3.5 dpc) were used as donors for blastocysts. Twelve to fifteen haploid ESCs were microinjected into

each blastocyst to produce chimeric embryo. After 1–4 h of culture, these manipulated embryos were transferred into the oviduct of psedudopregnant CD-1 mice at 0.5 or 2.5 dpc. Chimeras were identified by coat colors (Li et al., 2012).

Intracytoplasmic injection of phESCs and round spermatid

The phESC injection procedure was modified from a previously reported procedure (Li et al., 2016). In brief, mature MII oocytes were collected from the oviduct of super-ovulated 8-week-old female mice (B6D2F1, C57BL/6 × DBA/2). G0- or G1-phase phESCs with the deletion of imprinted regions were sorted with FACS and chosen as donors. Before the microinjection of phESC, oocytes were pre-activated by 10 mM $SrCl_2$ in calcium-free CZB medium for 30 min. Sorted phESCs were injected into oocytes separately to construct bimaternal embryos. The reconstructed embryos were activated by 10 mM $SrCl_2$ in calcium-free CZB medium at 37°C with 5% CO_2 for another 5 h. Completely activated embryos were washed and cultured in M16 medium (Sigma) at 37°C with 5% CO_2 as described (Dai et al., 2009). On the following day, bimaternal embryos at the 2-cell stage were transferred to the oviduct of psedudopregnant CD-1 mice at 0.5 dpc. To evaluate the development of bimaternal embryos, pregnant recipients were dissected on 13.5, 17.5, and 19.5 dpc, respectively. The round sperm injection (ROSI) experiment was carried out as a control with the described procedure (Li et al., 2012).

Coinjection of androgenetic haploid ESCs and sperm

Sperm of male 129S2/SvPasCrl mice were injected into MII oocytes by intracytoplasmic sperm injection (ICSI), followed by removal of spindle to generate an androgenetic haploid embryo. Reconstructed androgenetic haploid embryos were activated by 10 mM $SrCl_2$ in calcium-free CZB medium containing 5 mg/mL of cytochalasin B. One hour later, ahES cells (GFP + ahES cell at G0/G1 stage with 6 or 7 imprinted regions deleted) were injected to generate diploid reconstructed embryos. When the embryos developed to the 2-cell stage, derived embryos were activated by 10 mM SrCl2 in calcium-free CZB medium containing 5 mg/mL of cytochalasin B for 4 h and cultured in CZB at 37°C/5% CO2 for 28 h. They were then transferred into CD-1 pseudopregnant mice oviduct for development.

Establishment of diploid androgenetic ES cells

Sperm of male mice (B6.129 (Cg)-Gt (ROSA) 26Sortm4 (ACTB-tdTomato,-EGFP) Luo/J) were injected into MII oocytes by intracytoplasmic sperm injection (ICSI), followed by removal of spindle to generate an androgenetic haploid embryo. Reconstructed androgenetic haploid embryos were activated by 10 mM SrCl2 in calcium-free CZB medium containing 5 mg/mL of cytochalasin B. One hour later, GFP positive androgenetic haploid ESCs with 6 or 7 imprinted regions deleted (at G0/G1 stage) were injected into the reconstructed androgenetic haploid embryos to generate diploid reconstructed embryos. Diploid reconstructed embryos were activated by 10 mM SrCl2 in calcium-free CZB medium containing 5 mg/mL of cytochalasin B for 4 h and further cultured in CZB at 37°C/5% CO2 for 4.5 days. Blastocysts expressing both GFP and RFP were used to establish the ESCs.

Tetraploid embryo complementation of ESCs and diploid androgenetic ESCs

The generation of mice by tetraploid embryo complementation was carried out as previously described (Zhao et al., 2009). In brief, two-cell embryos were collected from oviducts of CD-1 females (white coat color) and electrofused to produce one-cell tetraploid embryos, which were then cultured in CZB media. Ten to fifteen ESCs or adESCs were injected into each tetraploid blastocyst and transferred to CD-1 pseudopregnant recipient females. Embryos derived from tetraploid blastocyst injection (4N) were dissected in handling media on E15.5 and the day of birth (E19.5), respectively.

RNA-seq library preparation and data analysis

Total RNA was extracted from tissues with TRIzol (Invitrogen). Following extraction, 1 μg of purified RNA was used for reverse transcription polymerase reaction each time (Invitrogen). For RNA-seq library construction, two rounds of PolyA+ tailed RNA purification were performed for each sample. Sequencing was performed on an Illumina HiSeq 2500 sequencer with 125 bp paired-end sequencing reaction. RNA-seq data analysis was performed with TopHat2 (version 2.1.1) and Cufflinks (version 2.2.1) using the UCSC mm9 annotation with default settings (Trapnell et al., 2012; Trapnell et al., 2010). Reads with unique genome location were used for differentially expressed gene analysis using Cuffdiff using default parameters. And two-fold changes and *P value* = 0.05 from Cuffdiff were used as the cutoff. The genes with no less than 1 FPKM in at least one sample were transformed by $\log_2$ and used to produce scatterplots by R.

RRBS library preparation and data analysis

The RRBS libraries were generated as previously described (Gu et al., 2011). Single-end or paired-end sequencing was performed on an Illumina HiSeq 2500 sequencer. In addition to the RRBS data produced in this experiment, other RRBS datasets, including WT oocyte and sperm (GSE61331), TTFs (GSE76238), and PGCs at different embryonic days (E10.5, E13.5, and E16.5) were downloaded from the GEO database or the European Nucleotide Archive or from Nodai genome database (http://www.nodai-genome.org/mouse.html?lang=en). All these data were analyzed together. Briefly, the sequencing reads were mapped to the mouse genome (version mm9) by Bismark v0.13.1 (Babraham Bioinformatics) after trimming by Trim Galore (Babraham Bioinformatics) with the "-rrbs" option. The methylation levels of covered cytosine sites were calculated by dividing the number of reported C with the total number of reported C and T. CpG sites covered by more than ten reads were used for the analysis. All heatmaps shown in

the manuscript were plotted with the heatmap.2 function of R. Histograms of methylation level distribution were drawn by ggplot2. The principal component analysis (PCA) were performed using prcomp function and showed by plot3D function in the R package. The clustering analyses were performed by kmeans function. The methylation levels of the CpG sites covered in all the samples were used in the analyses.

Open-field test

The apparatus consisted of a square-shaped arena (600 × 600 mm^2, length × width) constructed of blue plastic, and illuminated evenly at 15 lux^{50}. Test mice were placed facing the center of one wall and allowed to explore the apparatus for 10 min. The open field was subdivided into two virtual concentric squares (center region and all regions). The distance and the velocity spent in all regions were calculated.

Serum biochemical analysis

Blood samples were collected from the eyeground venous plexus of 12-month mice. Using a biochemical autoanalyzer (VITALAB, Merck, the Netherlands), serum biochemical analysis was carried out to determine the level of total protein, albumin, total bilirubin, aspartate transaminase (AST), alanine transaminase (ALT), glucose, cholesterol, triglyceride, blood urea nitrogen, creatinine, calcium, phosphorus, and lactic acid dehydrogenase etc. Serum cholesterol was also detected with Cholesterol Fluorometric Assay Kit (Cayman, 10007640) as described.

Micro-computed tomography image acquisition

Each full-term pup was subjected to hydrogel stabilization. To evaluate the pup mass and microarchitecture in bone among the WT, 6KO-, and 7KO-bipaternal mice, micro-CT was performed using the Inveon MM system (Siemens, Munich, Germany). Images with 8.82 μm pixel sizes were acquired under 60 kV of voltage, 300 μA of current and 1,500 ms of exposure time during the 360° rotational step. 2000 slices of images with voxel size of 8.82 μm × 8.82 μm × 8.82 μm were acquired. 3D reconstruction was performed using multimodal 3D visualization software (Inveon Research Workplace, SIEMENS, Munich, Germany).

MRI image acquisition

Axial, sagittial and coronal images of E19.5 full-term mice were acquired on a 7 Tesla MRI scanner (PharmScan 70/16 US, Bruker, Switzerland). A T2_TurboRare sequence was conducted to exhibit the contrast of tissue and interested organs.

Immunohistochemistry and HE staining

Full-term pups were fixed in 10% formalin for more than one week. The pups were then embedded in paraffin, and sliced to into 4 μm thick sections. After being baked at 37°C, they were placed at room temperature. Sections were deparaffinized in xylene (2 × 5 min), and rehydrated with successive 1-min washes in 100%, 96%, 80%, and 70% ethanol. The sections were stained with hematoxylin (2 min) and rinsed with distilled water, 0.1% hydrochloric acid in 50% ethanol, and distilled water for 15 min. They were then stained with eosin for 1 min, and rinsed again with distilled water. Following staining, the slides were dehydrated with 95% and 100% ethanol, dehydrated with xylene (2 × 5 min), mounted with coverslips, and photographed under a microscope.

QUANTIFICATION AND STATISTICAL ANALYSIS

Statistical analysis was performed using SPSS 17.0 statistical software. The Student's t test was used for statistical analysis. For all statistical analyses, a value of $p < 0.05$ was considered to be statistically significant.

DATA AND SOFTWARE AVAILABILITY

The sequencing data have been deposited in Genome Sequence Archive of Beijing Institute of Genomics, Chinese Academy of Sciences (http://gsa.big.ac.cn/) and NCBI (https://www.ncbi.nlm.nih.gov). The accession number for the sequencing data reported in this paper is CRA001069 or GSE120039. The list of software for data analysis and processing can be found in the Key Resources Table.